Vincenzina Barbera*, Andrea Bernardi*, Giulio Torrisi*,
Alessandro Porta*, Maurizio Galimberti*[1]

Controlled functionalization of sp^2 carbon allotropes for the reinforcement of diene elastomers

This paper reports functionalization reactions of sp^2 carbon allotropes, both nano- and nanostructured, able to introduce heteroatoms such as oxygen and nitrogen, without altering the bulk crystalline organization of the graphitic substrates. sp^2 carbon allotropes were: carbon black (CB), nanosized graphite with high surface area (HSAG), multiwalled carbon nanotubes (CNT). Reactions of carbon allotropes were performed with either KOH or hydrogen peroxide or a serinol derivative, 2-(2,5--dimethyl-1*H*-pyrrol-1-yl)-1,3-propanediol (serinolpyrrole, SP), in the absence of solvents or catalysts, by simply donating either thermal or mechanical energy. Sulphur cured composites with HSAG containing hydroxy groups (from the reaction with KOH) revealed better mechanical properties than composites from melt blending with pristine HSAG. CB functionalized with SP was able to promote reduction of Payne effect in compounds based on CB and silica.
Keywords: sp^2 carbon allotrope, functionalization, NR latex.

Kontrolowana funkcjonalizacja alotropów węgla sp^2 w celu wzmocnienia elastomerów dienowych

W artykule przedstawiono reakcje funkcjonalizacji alotropów węgla sp^2, zarówno nano-, jak i nanostrukturalnych, zdolnych do wprowadzania heteroatomów, takich jak tlen i azot, bez zmiany struktury krystalicznej materiałów grafitowych. Alotropami węgla sp^2 były: sadza (CB), grafit nanokrystaliczny o dużej powierzchni (HSAG), wielowarstwowe nanorurki węglowe (CNT). Reakcje alotropów węgla przeprowadzono za pomocą KOH lub nadtlenku wodoru lub pochodnej serinolu, 2-(2,5-dimetylo-1*H*-pirol-1-ylo)-1,3-propanodiolu (serinolopirolu, SP), w nieobecności rozpuszczalników lub katalizatorów, po prostu dostarczając energii cieplnej lub mechanicznej. Kompozyty utwardzane siarką z grupami hydroksylowymi HSAG (z reakcji z KOH) wykazały lepsze właściwości mechaniczne niż kompozyty uzyskane w wyniku mieszania w stanie stopionym z czystym HSAG. CB funkcjonalizowana za pomocą SP była w stanie zapewnić redukcję efektu Payne'a w mieszankach opartych na CB i krzemionce.
Słowa kluczowe: alotrop węgla sp^2, funkcjonalizowanie, lateks NR.

1. Introduction

sp^2 carbon allotropes are fundamental materials for the reinforcement of rubber. Carbon black (CB) [1, 2] is the most important filler and has been used for over a century: it is nanostructured filler, made by primary nanometric particles, fused together to form micron-sized aggregates. Over the last decades, nanofillers such as carbon nanotubes (CNT) [3–6], graphene (G)

*Politecnico di Milano,
Department of Chemistry,
Materials and Chemical
Engineering "G. Natta",
Via Mancinelli 7,
20131 Milano, Italy
[1]e-mail:
maurizio.galimberti@polimi.it

Dr Vincenzina Barbera – Since May 16, 2013 Post-Doc Research Fellow, department of Chemistry, Material and Chemical Engeneering, Politecnico di Milano. She has been leaded by Professor Maurizio Stefano Galimberti. The topic of the research activity was "Materiali nanostrutturati e sintesi e caratterizzazione di monomeri e polimeri a partire da building block C3". In 2009 she received Master's Degree in "Chimica e Tecnologie Farmaceutiche" (Medicinal Chemistry) Università degli studi di Catania, Catania, Italy and in 2013 PhD in Pharmaceutical Sciences, Università degli studi di Catania, Catania, Italy. Author or co-author of 17 publications on journals. 1 chapters on books, 7 publications on proceedings, 29 oral communications at meetings, 4 Posters presented at meetings and 6 patent applications. In 2017 she was awarded first place in "switch2product Innovation challenge" for the project "Lightweight materials".

and graphene related materials [7–11] have steadily increased their importance [12–14]. Nanofillers can be separated in individual nanometric particles and large interfacial area is established with the polymer matrix, with significant impact on the material properties. A large variety of carbon nanofillers is nowadays available [15] and it has been recently reported [16]: "Have we reached a point in 2016 that would cause us to declare the "End of Carbon Science" ? (…) the answer is "no". There are various new allotropes to be synthesized, and there are major challenges in combining our basic low-dimensional forms into more complex 3D architectures."

It is acknowledged that, in rubber compounds for large scale applications, nanofillers will be used in partial replacement of carbon black: hybrid filler systems will be developed. Indeed, hybrid filler systems based on sp^2 carbon allotropes have been carefully investigated [17–19] and reviews are already available [20]. For both nanometric and nanostructured fillers, as well as for the hybrid filler systems, common correlation has been demonstrated between mechanical reinforcement and polymer-filler interfacial area, calculated as the product of volume fraction, density and surface area: experimental points lie on a sort of master curve in a graph reporting the initial modulus as a function of the interfacial area [21]. It is nowadays clear that most of the effects brought about by nanofillers are due to their nanosize and shape: indeed, anisometric particles of CNT and GRM lead to anisotropic mechanical properties [22]. Anisotropic properties of elastomer composites based on either nanostructured or nanometric fillers have been comparatively investigated [23].

Knowledge on sp^2 carbon allotropes, both nanometric and nanostructured, is thus steadily increasing, though it appears prevailingly focused on mechanical aspects of elastomeric composites. There is a lack of comparative studies on the chemical reactivity of such carbon fillers. Chemical reactions on sp^2 carbon allotropes would be aimed at introducing functional groups, favoring their compatibility with different environments, such as the elastomeric phases. There is a rich literature on the functionalization of carbon allotropes, as summarized in [24] and, for GRM in particular, in [25]. As mentioned above, CB is the most important carbon filler. Many scientific and technological approaches have been developed to introduce functional groups on CB [26–35)]. Carbon/silicon dual phase was obtained

through the so called cofuming technology [27–28], CB was treated with ozone [29–33], polysulfide [34], triazole [35]. Plasma treatment was applied to CB [36] as well as to carbon nanotubes [37]. Common objective of such technologies was to promote the interaction of CB with the polymer matrix. However, the mentioned technologies appear to be specific for the type of carbon allotrope. Moreover, some (if not most) of them imply the use of complex procedures, harsh reaction conditions, dangerous when not toxic reagents.

The research activity, which led to the results reported in the present paper, was aimed at preparing functionalized carbon allotropes through sustainable chemistry, adopting a facile, sustainable and versatile functionalization method, suitable for all the families of sp^2 carbon allotropes. Studies have been performed on the following carbon allotropes: carbon black, nanosized graphite with high surface area and shape anisotropy [38], multiwalled carbon nanotubes. Carbon allotropes were reacted with either KOH or with H_2O_2, with the aim to introduce oxygenated functional groups. Carbon allotropes functionalization was as well performed with the molecule shown in Figure 1: 2-(2,5-dimethyl-1*H*-pyrrol-1-yl)-1,3-propanediol (serinolpyrrole, SP).

Such molecule derives from 2-amino-1,3-propane--diol (serinol, S), a molecule endowed with chemoselectivity, which can be prepared through chemical synthesis from glycerol or dihydroxyacetone or can be obtained from renewable sources [39].

Some functionalization reactions of carbon allotropes with the above reported methods have been already reported: HSAG was reacted with SP [24, 40] and KOH [41] and CB with SP [24]. In this paper, for the first-time comparative studies for the functionalization of HSAG, CB and CNT are discussed. In particular, data obtained with H_2O_2 as the oxidizing agent are for the first time shown. Although the research is still in progress and only some data are available, experimental procedures, reactions' efficiency, adducts' characteristics are presented. Functionalized carbon allotropes have been characterized through thermogravimetric analysis (TGA), Fourier transformed infrared spectroscopy (FT-IR), Raman spectroscopy, wide angle X-ray diffraction (WAXD). Elastomers composites based on natural rubber (NR) and functionalized HSAG and carbon black are presented. Structural investigation, vulcanization behaviour and dynamic-mechanical properties are discussed.
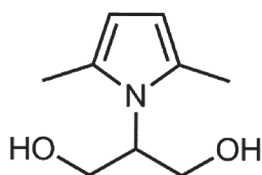

Fig. 1. 2-(2,5-dimethyl-1*H*-pyrrol-1-yl)-1,3-propanediol (serinolpyrrole, SP)
Rys. 1. 2-(2,5-dimetylo-1*H*-pirol-1-ylo)-1,3-propanodiol (serinolopirol, SP)

2. Experimental

2.1. Materials

2.1.1. Carbon allotropes

Carbon Black N326 (CB) was from Cabot, with the following characteristics: 30 nm as mean diameter of spherical primary particles; BET surface area of 77m^2/g; 85 mL of absorbed DBP / 100 grams of CB [42]. Multi-wall Carbon Nanotubes were NANOCYL® NC7000™ series, with carbon purity of 90%, average length of about 1.5 μm, BET surface area of 275 m^2/g, 316 mL of absorbed DBP / 100 grams of CNT. High surface area graphite (HSAG) was Nano24 from Asbury Graphite Mills Inc., with carbon content reported in the technical data sheet of at least 99 wt%. Chemical composition determined from elemental analysis was, as wt%: carbon 99.5, hydrogen 0.4, nitrogen 0.1, oxygen <0.05. BET surface area was 330 m^2/g and DBP absorption was 162 mL/100 g.

2.1.2. Chemicals for functionalization reactions

Reagents and solvents commercially available were purchased and used without further purification: 2,5-hexandione (Merck – Schuchardt), 2-amino-1,3--propanediol (kindly provided by Bracco), H$_2$O$_2$ 30% (w/w) in H$_2$O (Sigma-Aldrich), KOH pellets pure (Sigma-Aldrich).

2.1.3. Rubbers

Synthetic poly(1,4-*cis*-isoprene) (IR) was SKY3 from Nizhnekamskneftechim Export, with 70 Mooney Units (MU) as Mooney viscosity ($M_L(1+4)100°C$), synthetic poly(1,3-butadiene) (BR) was Neocis BR 40 from Versalis, with a 43 Mooney Viscosity ($M_L(1+4)100°C$). Poly(1,4-cis-isoprene) from *Hevea brasiliensis* (NR) (EQR-E.Q. Rubber, BR-THAI, Eastern GR. Thailand – Chonburi) had trade name SIR20 and 73 Mooney Units (MU) as Mooney viscosity ($M_L(1+4)100°C$).

Latex from *Hevea brasiliensis*: STR20 from Eastern GR Thailand – Chonburi (NR-L).

2.1.4. Chemicals for elastomeric compounds' preparation

Silica was Zeosil 1115 (industrial grades for tire applications) from Solvay, with 115 m^2/g as specific surface area determined trough nitrogen absorption (BET). The following ingredients were used as received: bis(3-triethoxysilylpropyl)tetrasulfide (TESPT) (Si69 Evonik), ZnO (Zinc Oxide), Stearic acid (Sogis), (1,3--dimethylbutyl)-*N'*-*p*henyl-*p*-phenylenediamine (6PPD) (Crompton), Sulphur (Solfotecnica), *N*-tert-butyl-2--benzothiazyl sulfenamide (TBBS) (Flexsys).

2.2. Functionalization reactions

2.2.1. Reaction of HSAG with KOH. Synthesis of G–OH

The reaction of HSAG with KOH was performed using a planetary ball mill S100 from Retsch, having the grinding jar moving in a horizontal plane, with a volume of 0.3 L. The grinding jar was loaded with 6 ceramic balls having a diameter of 20 mm. HSAG (1 g, 14 mmol of benzene rings), KOH powder (20 g, 356 mmol) and H$_2$O (6.5 mL) were put into the jar, that could rotate at 300 rpm, at room temperature, for 10 hours. After this time, the mixture was placed in a Büchner funnel with a sintered glass disc and repeatedly washed with distilled water (6 × 100 mL) under vacuum. Finally, the obtained solid was put in an oven to remove excess water. 0.65 g of black powder were obtained. ATR-FTIR ν$_{max}$ 3390 (O–H stretch, broad), 1396 (in plane O–H bend), 1120 (C–O stretch), 983 (C=C bend), 850 (out of plane, =C–H bend, monosubst.) cm^{-1}.

2.2.2. Reaction of CB with KOH. Synthesis of CB–OH

The synthesis of hydroxy-carbon black (CB–OH) was performed using a planetary ball mill S100 from Retsch, having the grinding jar moving in a horizontal plane, with a volume of 0.3 L. The grinding jar was loaded with 6 ceramic balls having a diameter of 20 mm. Carbon black (10 g, 139 mmol), KOH powder (2 g, 35.6 mmol) and H$_2$O (20 mL) were put into the jar, that was allowed to rotate at 300 rpm, at room temperature, for 10 hours. After this time, the mixture was placed in a Büchner funnel with a sintered glass disc and repeatedly washed with distilled water, up to neutral pH, under vacuum. Finally, the obtained solid was put in an oven to remove excess water. 9.27 g of black powder were obtained.

2.2.3. Reaction of CNT with KOH. Synthesis of CNT–OH

In a 500 mL round bottom flask equipped with a magnetic stirrer were poured in sequence carbon

nanotubes (10 g, 139 mmol), KOH powder (2 g, 35.6 mmol) and H_2O (25 mL). The mixture was left to stir at 100°C for 3 hours. After this time, the reaction mixture was cooled down to room temperature and removed from the flask using deionized water. The resulting suspension was poured in a Büchner funnel and washed with water under vacuum up to neutral pH. The obtained solid was put in a stove for 6 hours to remove excess water. 9.13 g of black powder were obtained.

2.2.4. Reaction of HSAG with H_2O_2. Synthesis of G–Ox (Method A)

Pristine HSAG (1 g, 13.9 mmol) was poured in a 50 mL round bottomed flask, equipped with a magnetic stirrer. H_2O_2 was added to the flask using a pipette. The mixture was left to stir at 70°C for 3 hours. After this time, the flask was cooled down at room temperature and 5 mL of H_2O were added to dilute the H_2O_2. The resulting mixture was removed from the flask using deionized water and the resulting suspension was poured in a Büchner funnel and washed with water under vacuum up to neutral pH. The obtained solid was put in a stove for 6 hours to remove excess water. 0.90 g of powder were obtained.

2.2.5. Reaction of HSAG with H_2O_2. Synthesis of G–Ox (Method B)

Pristine HSAG (1 g, 13.9 mmol) was poured in a 50 mL round bottomed flask, equipped with a magnetic stirrer. H_2O_2 was added to the flask using a pipette. The mixture was left to stir at room temperature for 24 hours. After this time, the flask was cooled down at room temperature and 5 mL of H_2O were added to dilute the H_2O_2. The resulting mixture was removed from the flask using deionized water and the resulting suspension was poured in a Büchner funnel and washed with water under vacuum up to neutral pH. The obtained solid was put in a stove for 6 hours to remove excess water. 0.89 g of powder were obtained.

2.2.6. Reaction of CB with H_2O_2. Synthesis of CB–Ox (Method A)

In a 50 mL round bottom flask equipped with a magnetic stirrer was poured the pristine carbon black (1 g, 13.9 mmol). The H_2O_2 has been added to the flask using a pipette. The mixture was left to stir at 70°C for 3 hours. After this time, the flask was cooled down at room temperature and 5 mL of H_2O were added to dilute the H_2O_2. The resulting mixture was removed from the flask using deionized water and

the resulting suspension was poured in a Büchner funnel and washed with water under vacuum up to neutral pH. The obtained solid was put in a stove for 6 hours to remove excess water. 0.85 g of powder were obtained.

2.2.7. Reaction of CB with H_2O_2. Synthesis of CB–Ox (Method B)

In a 50 mL round bottom flask equipped with a magnetic stirrer was poured the pristine carbon black (1 g, 13.9 mmol). The H_2O_2 has been added to the flask using a pipette. The mixture was left to stir at room temperature for 24 hours. After this time, the flask was cooled down at room temperature and 5 mL of H_2O were added to dilute the H_2O_2. The resulting mixture was removed from the flask using deionized water and the resulting suspension was poured in a Büchner funnel and washed with water under vacuum up to neutral pH. The obtained solid was put in a stove for 6 hours to remove excess water. 0.95 g of powder were obtained.

2.2.8. Reaction of CNT with H_2O_2. Synthesis of CNT–Ox (Method A)

In a 50 mL round bottom flask equipped with a magnetic stirrer was poured the pristine carbon nanotubes (1 g, 13.9 mmol). The H_2O_2 has been added to the flask using a pipette. The mixture was left to stir at 70°C for 3 hours. After this time, the flask was cooled down at room temperature and 5 mL of H_2O were added to dilute the H_2O_2. The resulting mixture was removed from the flask using deionized water and the resulting suspension was poured in a Büchner funnel and washed with water under vacuum. The obtained solid was put in a stove for 6 hours to remove excess water. 1.05 g of powder were obtained.

2.2.9. Reaction of CNT with H_2O_2. Synthesis of CNT–Ox (Method B)

In a 50 mL round bottom flask equipped with a magnetic stirrer was poured the pristine carbon nanotubes (1 g, 13.9 mmol). The H_2O_2 has been added to the flask using a pipette. The mixture was left to stir at room temperature for 24 hours. After this time, the flask was cooled down at room temperature and 5 mL of H_2O were added to dilute the H_2O_2. The resulting mixture was removed from the flask using deionized water and the resulting suspension was poured in a Büchner funnel and washed with water under vacuum up to neutral pH. The obtained solid was put in a stove for 6 hours to remove excess water. 0.99 g of powder were obtained.

2.2.10. Synthesis of 2-(2,5-dimethyl-1H-pyrrol-1-yl)-1,3-propanediol (SP)

A mixture of 2,5-hexanedione (37.67 g, 0.33 mol) and serinol (30.06 g, 0.33 mol) was poured into a 100 mL round bottomed flask equipped with magnetic stirrer. The mixture was then stirred, at room temperature, for 6 h. The resulting compound 4a,6a-dimethyl-hexahydro-1,4-dioxa-6b-azacyclopenta[cd]pentalene (HHP) was characterized through ^{1}H NMR and the yield was estimated to be 99%.

^{1}H NMR (400 MHz, DMSO-d6, δ in ppm): 1.28 (s, 6H); 1.77 (m, 2H); 1.93 (m, 2H); 3.60 (m, 4H); 3.94 (q, 1H).

The product mixture obtained from the synthesis of HHP was kept under vacuum for 2 h and then heated to 180°C for 60 min. After distillation under reduced pressure at 130°C and 0.1 mbar, SP was isolated as yellow oil with 96% yield.

^{1}H NMR (400 MHz, DMSO-d6, δ in ppm): 2.16 (s, 6H, –CH$_3$ at C-2,5 of pyrrole moiety); 3.63 (m, 2H, CH$_2$OH); 3.76 (m, 2H, CH$_2$OH); 4.10 (quintet, 1H, at C-3 of diol); 4.73 (t, 2H, CH$_2$OH); 5.55 (s, 2H, C-3,4 of pyrrole moiety).

2.2.11. Synthesis of HSAG–SP adduct

In a 100 mL round bottom flask there were put in sequence HSAG (5 g, 69.4 mmol) and acetone (15 mL). The suspension was sonicated for 15 min, using a 2 L ultrasonic bath. In 5 mL of acetone, 0.5 g of SP (2.9 mmol) were added. The resulting suspension was sonicated for 15 min. The solvent was removed under reduced pressure. The black powder of HSAG/SP was poured into a 100 mL round bottomed flask equipped with magnetic stirrer and was heated at 180°C for 2 h. After this time, the mixture was placed in a Büchner funnel with a sintered glass disc, thoroughly washed with acetone and then recovered and weighed (96% yield).

2.2.12. Synthesis of CB–SP adduct

In a 100 mL round bottom flask there were put in sequence CB N326 (5 g, 69.4 mmol) and acetone (15 mL). The suspension was sonicated for 15 min, using a 2 L ultrasonic bath. In 5 mL of acetone, 0.5 g of SP (2.9 mmol) were added. The resulting suspension was sonicated for 15 min. The solvent was removed under reduced pressure. The black powder of CB/SP was poured into a 25 mL round bottomed flask equipped with magnetic stirrer and was heated at 180°C for 2 h. After this time, the mixture was placed in a Büchner funnel with a sintered glass disc, thoroughly washed with acetone and then recovered and weighed (82% yield).

2.2.13. Synthesis of CNT–SP adduct

In a 100 mL round bottom flask there were put in sequence CNT Nanocyl7000 (5 g, 69.4 mmol) and acetone (15 mL). The suspension was sonicated for 15 min, using a 2 L ultrasonic bath. In 5 mL of acetone, 0.5 g of SP (2.9 mmol) were added. The resulting suspension was sonicated for 15 min. The solvent was removed under reduced pressure. The black powder of CNT/SP was poured into a 25 mL round bottomed flask equipped with magnetic stirrer and was heated at 180°C for 2 h. After this time, the mixture was placed in a Büchner funnel with a sintered glass disc, thoroughly washed with acetone and then recovered and weighed (92% yield).

2.3. Dispersion of CA adducts in natural rubber latex

2.3.1. Dispersion of G–OH in natural rubber latex

The natural rubber used was poly(1,4-*cis*-isoprene) from *Hevea brasiliensis*. For each compound an aqueous suspension of hydroxy–graphite (G–OH) (1% wt) was prepared in a 1 L becker, then stirred at room temperature with magnetic stirrer for 15 min and sonicated for 15 min. Meanwhile in a 1 L Beckerit was poured latex and water in order to dilute latex 1:3 vol / vol. The obtained suspension of latex was stirred at room temperature with magnetic stirrer for 10 min. After that, the aqueous suspension of hydroxy–graphite (G–OH) (1% wt) was added to the latex suspension and stirred again with magnetic stirrer for 15 min, then sonicated for 15 min. Subsequently, during the stirring, the coagulating agent (an aqueous solution – 2% of sulphuric acid) was added. The coagulated compound was cut into small pieces and washed with water until it reached neutral pH and dried at room temperature for several days.

2.3.2. Dispersion of HSAG–SP adduct in natural rubber latex

The natural rubber used was poly(1,4-*cis*-isoprene) from *Hevea brasiliensis*. 0.05 g of HSAG–SP adduct was added into 10 mL of water. The dispersion was then sonicated in a 2 L ultrasonic bath with a power of 260 Watts for 15 minutes. A dispersion was obtained, in which no presence of powders was noted. This dispersion was added to 0.84 grams of latex. The dispersion obtained was stirred with magnetic stirrer

for 60 minutes and then sonicated for 1 minute. Precipitation was then performed by adding a 0.1 M sulfuric acid solution. A composite material based on natural rubber containing HSAG–SP was obtained.

2.3.3. Dispersion of CB–SP adduct in natural rubber latex

The natural rubber used was poly(1,4-*cis*-isoprene) from *Hevea brasiliensis*. 0.05 grams of CB–SP adduct was added to 10 mL of water. The dispersion was then sonicated in a 2 L ultrasonic bath with a power of 260 Watts for 15 minutes. A solution was obtained, in which no presence of powders was noted. This solution was added to 0.84 grams of latex. The dispersion obtained was stirred with magnetic stirrer for 60 minutes and then sonicated for 1 minute. Precipitation was then performed by adding a 0.1 M sulfuric acid solution. A homogeneous and continuous composite material based on natural rubber containing CB–SP was obtained.

2.4. Preparation of elastomer composites

2.4.1. Preparation of composites based on NR and G–OH

Six different composites were prepared with different amount (phr) of G–OH: 0, 3, 6, 9, 12, 15. The preparation of the composites was performed using an internal mixer (Brabender®) with an inner chamber of 12 cc. A standard procedure was adopted for all the preparations. Formulation of composites are reported in Table 1.

NR/G–OH masterbatch (prepared as described in 2.4.1) was masticated for 1 min at 80°C, then stearic acid and zinc oxide were added and mixed for 2 min, and finally 6PPD, TBBS and sulphur were added, and further mixing was performed for 2 min.

2.4.2. Preparation of composites based on IR/BR, CB, silica and CB–SP

Recipes are shown in Table 2.

Table 2. Recipes of composites (a), (b) with CB–SP, containing IR, BR as the rubbers and CB, silica as the fillers [a, b]
Tabela 2. Receptury kompozytów (a) i (b) zawierających kauczuki IR, BR oraz CB i krzemionkę jako napełniacze[a, b]

Ingredient	Composite	
	(a)	**(b)**
IR	50.0	50.0
BR	50.0	50.0
CBN326	25.0	20.0
CB–SP[c]	0.0	5.5
Silica	25.0	25.0
TESPT	2.0	2.0

[a] amounts in phr
[b] Other ingredients: ZnO 4.0, Stearic acid 2.0, 6PPD 2.0, S 1.5, TBBS 1.8
[c] amount of SP on CB 1 : 10 mass

2.4.2.1. Procedure for the preparation of elastomeric compounds without CB–SP

16.12 g of poly(1,3-butadiene) (BR) and 16.12 g of poly(1.4-*cis*-isoprene) (IR) were fed into a Brabender® internal mixer with a mixing chamber with a volume of 50 cc and masticated at 145°C for 1 minute. 8.06 g of silica and 1.09 g of silane TESPT were added and mixed for 4 minutes. The obtained compound was unloaded at 145°C. The composite thus prepared was then fed into the internal mixer at 80°C, masticated for 1 minute, then 8.06 g of CB N326 were added and mixed for a further 4 minutes, then unloaded at 80°C. This composite was fed again into the internal mixer at 50°C, adding 1.29 g

Table 1. Formulations of composites based on NR and G–OH
Tabela 1. Skład kompozytów na podstawie NR i G–OH

Ingredient	G-OH_0	G-OH_4	G-OH_7	G-OH_10	G-OH_12	G-OH_15	G-OH_25
NR	100	100	100	100	100	100	100
G-OH theoretical	0	3	6	9	12	15	25
G-OH experimental	0	3.7	6.5	9.5	12.3	15.1	n.d.

[1] Amounts of ingredients are expressed in phr
[2] Other ingredients: ZnO 4 phr, Stearic acid 2 phr, 6PPD 2 phr, S 3 phr, TBBS 1.8 phr.

of ZnO, 0.64 g of stearic acid and 0.64 g of 6PPD and mixed for 2 minutes. 0.48 g of sulfur and 0.58 g of *N-t*-butyl-2-benzothiazole sulfenamide (TBBS) were then added, mixing for a further 2 minutes. The composite was unloaded at 50°C.

2.4.2.2. Procedure for the preparation of elastomeric compounds with CB–SP

The same procedure was followed, except that 5 phr of CB were replaced by 5.5 phr (1.58 g) of CB/SP (CB: 5 phr, SP: 0.5 phr).

2.5. Characterization

2.5.1. Characterization of functionalized sp² carbon allotropes

2.5.1.1. Boehm titration

It was performed to quantitatively determine the content of oxygenated surface groups. In a typical experiment, 0.05 g of the carbon allotrope were dispersed in 50 mL of a 0.05 M NaOH solution and water removal was performed (full procedure described below). After stirring at room temperature for 24 h, the mixture was filtrated. The removal of the solid carbon allotrope from the solution is essential to avoid the reaction of deprotonated groups on carbon allotrope surface with HCl. A part of the solution (10 mL) was mixed with a water solution of HCl (0.05 N, 20 mL). The obtained mixture was titrated using a 0.05 M solution of NaOH.

CO₂ removal with N₂
CO_2 was removed from solution immediately before the titration: samples were poured in 40 mL glass vials equipped with a glass septum lids. N_2 was bubbled into the vial through a needle submerged in the solution. Bubbling rate was less than 1 mL/min. The time of degasification was 24 h. After degasification, the samples were transferred to a beaker that had been purged with the inert gas and covered with Parafilm®, to prevent absorption of atmospheric CO_2.

2.5.1.1.1. Boehm titration on G–OH sample

100 mg of G–OH were poured in a becker with 50 mL of NaOH 0.0492 M. The mixture was left to stir at room temperature for 24 hours. After this time, the suspension was filtrated. 10 mL of the filtered product was withdrawn with a pipette and placed in a becker with the addition of 20 mL of HCl 0.05 M and 2 drops of phenolphthalein. The solution was titrated with NaOH 0.0492 M.

$$X_C = \frac{M_{NaOH}\left(y\,\text{ml} + \frac{V_{NaOH}}{5}\right) - M_{HCl}(V_{HCl})}{\frac{m_{G-OH}}{5}} \qquad (1)$$

2.5.1.2. Infrared spectroscopy

FT-IR absorption spectra were recorded in transmission mode using a diamond anvil cell (DAC) coupled with a Thermo Electron FT-IR Continuµm IR microscope (resolution: 4 cm⁻¹; scans: 128).

2.5.1.3. Raman spectroscopy

Raman spectra of powder samples were recorded with a Horiba Jobin Yvon's LabRam HR800 dispersive Raman spectrometer equipped with an Olympus BX41 microscope and a 50X objective (resolution: 2 cm⁻¹; acquisition time: 30 seconds and 4 accumulation). The excitation line at 514.5 nm of an Ar⁺ laser was kept at 0.5 mW to prevent possible photo induced thermal degradation of the samples. Each Raman spectrum reported was obtained as average of four spectra recorded in different points of the sample.

2.5.1.4. Wide angle X-ray diffraction

WAXD patterns were obtained in reflection, with an automatic Bruker D8 Advance diffractometer, with nickel filtered Cu–K$_\alpha$ radiation. Patterns were recorded in 4° – 80° as the 2θ range, being 2θ the peak diffraction angle. Distance between crystallographic planes of HSAG was calculated from the Bragg law. The D_{hkl} correlation length, in the direction perpendicular to the *hkl* crystal graphitic planes, was determined applying the Scherrer equation:

$$D_{hkl} = \frac{K \cdot \lambda}{\beta_{hkl} \cdot \cos\theta_{hkl}} \qquad (2)$$

where K is the Scherrer constant, λ is the wavelength of the irradiating beam (1.5419 Å, Cu-K$_\alpha$), β_{hkl} is the width at half height, and θ_{hkl} is the diffraction angle. The instrumental broadening, b, was determined by obtaining a WAXD pattern of a standard silicon powder 325 mesh (99%), under the same experimental conditions. The width at half height $\beta_{hkl} = (B_{hkl} - b)$ was corrected, for each observed reflection with $\beta_{hkl} < 1°$, by subtracting the instrumental broadening of the closest silicon reflection from the experimental width at half height, β_{hkl}.

2.5.1.5. Thermogravimetric analysis

TGA tests under flowing N_2 (60 mL/min) were performed with a Mettler TGA SDTA/851 instrument according to the standard method ISO9924-1. Samples (10 mg) were heated from 30 to 300°C at 10°C/min, kept at 300°C for 10 min, and then heated up to 550°C at 20°C/min. After being maintained at 550°C for 15 min, they were further heated up to 700°C and kept at 700°C for 30 min under flowing air (60 mL/min).

2.5.2. Characterization of elastomer composites

2.5.2.1. Crosslinking reaction

Crosslinking reaction was performed at 170°C for 10 min for composites based on poly(1,4-*cis*-isoprene). A Monsanto oscillating disc rheometer (MDR 2000) (Alpha Technologies, Swindon, UK) was used, determining the minimum modulus M_L, the maximum modulus M_H, the modulus M_{final} at the end of the crosslinking reaction, the time t_{s1} required to have a torque equal to $M_L + 1$, the time t_{90} required to achieve 90 % of the maximum modulus M_H (i.e. to achieve the optimum of crosslinking) and the so called reversion, i.e. the relative decrease of the modulus at the end of the crosslinking reaction:

$$(M_H - M_{final})/(M_H - M_L) \cdot 100.$$

2.5.2.2. Crosslinking and dynamic mechanical characterization

Crosslinking reaction was studied at 170°C with a Monsanto R.P.A 2000 rheometer, determining the minimum modulus M_L the maximum modulus M_H final at the end of crosslinking reaction, the time t_{s1} the time required to have a torque equal to M_L+1, the time t_{90} required to achieve 90% of the maximum modulus M_H.
Dynamic shear moduli were then measured at 50°C, with a sinusoidal strain at 1 Hz of frequency, in a strain amplitude ranging from 0.1 % to 25%.

2.5.2.3. Stress-strain tests

The stress-strain behavior of the cured composites was investigated on a universal tensile testing machine (Zwick/ Roll 2010) at a strain rate of 200 mm/min. S2 tensile specimens were prepared in accordance with DIN 53 504 from vulcanized flat sheets. The samples were fixed in pneumatic grips and stretched at constant feed until tensioned to failure. Ultimate tensile strength, modulus at 100% elongation and elongation at break has been determined.

3. Results and discussion

3.1. Functionalization of carbon allotropes

Reactions of carbon allotropes with KOH were performed as summarized in Figure 2, as described in detail in the experimental part.
In brief, the carbon allotrope and KOH powder were simply mixed and either mechanical or thermal energy were given, by using a planetary ball mill or by simply heating. First experiments performed with HSAG have been reported elsewhere [41]. KOH/CA mass ratios were in the range from 20:1 to1:5. In this paper, samples obtained with 1:1 as the mass ratio are discussed. The oxidized carbon allotropes were isolated after careful washing, until neutral pH was achieved. This functionalization method is simple indeed. The critical step could be the neutralization of the carbon allotrope after the reaction: optimization is still to be performed, though the neutralization procedure is not that troublesome, when little amount of KOH is used. The number of functional groups introduced on the carbon allotrope was estimated by means of Boehm titration (see the Experimental part), a method able to detect the amount of acidic groups. Values from the titrations are shown in Table 3. They are: 10.0, 2.0 and 3.0 mmol/g for HSAG, CB and CNT, respectively. The high value found for HSAG could be ascribed to the large surface area (330 m^2/g). However, this interpretation does not appear reliable for CNT, which have a large surface area (275 m^2/g) but a relatively low number of functional groups. In a previous publication
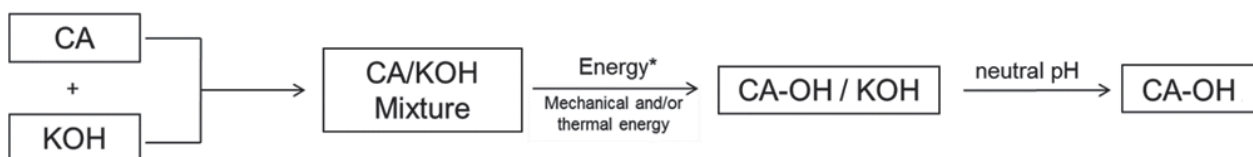
Fig. 2. Block diagram for the preparation of CA–OH
Rys. 2. Schemat blokowy przygotowania CA–OH

[43], it was hypothesized an aromatic nucleophilic substitution by KOH on the edge benzene e rings of the graphene layers. In the light of such mechanism, HSAG should be more reactive, for the larger amount of edges available for the hypothesized reaction.

In the text below, FT-IR, WAXD and Raman characterizations of G–OH sample are shown, in comparison with HSAG samples after the reaction with H_2O_2 and SP.

Reactions of carbon allotropes with H_2O_2 were performed as summarized in Figure 3 and as described in detail in the experimental part.

In brief, the carbon allotrope and H_2O_2 were stirred, in absence of solvents (other than water) and catalysts, either at room temperature or at 70°C, for either 24 or 3 hours, respectively. The oxidized carbon allotropes were isolated by washing until neutral pH. The number of functional groups on the carbon allotropes was estimated by means of Boehm titration. At higher temperature, though in a shorter time, larger number of functional groups were added onto the carbon allotrope. Data in Table 3 refer to reactions performed at 70°C. The relative number of functional groups appears to be different from the one detected in the case of carbon allotropes reacted with KOH. To account for the larger number of functional groups on CB, it could be taken into consideration that pristine CB contains a clearly detectable amount of alkenylic and oxygenated groups, which easily undergo oxidation by H_2O_2.

Serinolpyrrole was synthesized through the Paal–-Knorr reaction [43, 45] of 2-amino-1,3-propanediol with 2,5-hexanedione (HD), reproducing the synthesis already reported in previous publications [24, 40]. The synthesis, performed in the absence of solvent and catalyst, is summarized in the Scheme of Figure 4.

Water was the only by-product of the reaction, which was characterized by high atom economy, 82.4% and by a yield in the range from 95% and 99%. SP is a colorless or light yellow liquid (at room temperature and 1 atm pressure), with very high solubility in water.

Reactions of carbon allotropes with serinolpyrrole were performed as summarized in Figure 5 and as described in detail in the Experimental Part. Experiments and results have been reported elsewhere, performing the reaction of SP with HSAG [24, 44] and with CB [24].

Table 3. Number of functional groups of functionalized carbon allotropes from Boehm titration

Tabela 3. Liczba grup funkcyjnych funkcjonalizowanych alotropów węglowych na podstawie miareczkowania Boehma

Sample	Acidic functional groups [mmol/g]
Reaction with KOH	
HSAG	10.0
CB	2.0
CNT	3.0
Reaction with H_2O_2[a]	
HSAG	3.1
CB	5.8
CNT	3.2
Reaction with SP	
HSAG	6.3
CB	7.7
CNT	2.6

[a] reaction performed at 70°C
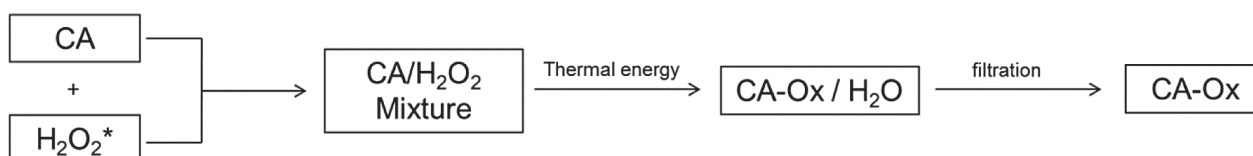
Fig. 3. Block diagram for the preparation of CA–Ox
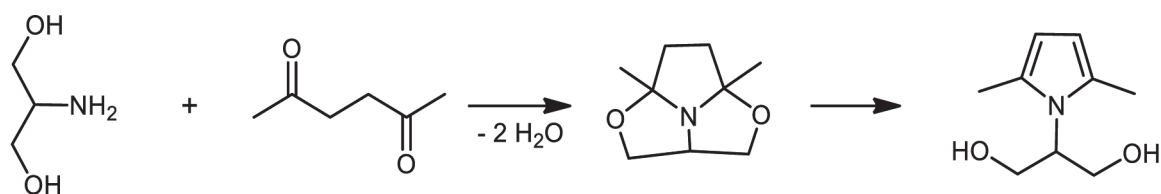**Rys. 3.** Schemat blokowy przygotowania CA–Ox

Fig. 4. Reaction of serinol with 2,5-hexanedione to give serinolpyrrole
Rys. 4. Reakcja serinolu z 2,5-heksanodionem prowadząca do otrzymania serinolopirolu

Fig. 5. Block diagram for the preparation of CA–SP adducts
Rys. 5. Schemat blokowy przygotowania adduktów CA–SP

In brief, adducts were prepared by simply mixing a carbon allotrope and SP and donating either thermal or mechanical energy, in the absence of solvents or other substances. The number of functional groups on the carbon allotropes was estimated by means of Boehm titration and TGA. Data from Boehm titration are in Table 3. It could be commented that allotropes with larger surface area (HSAG, CNT) have larger number of functional groups. Data in Table 4 come from TGA analysis.

TGA was performed under nitrogen on the CA–SP adducts, as explained in detail in the experimental part. Data are also reported for pristine HSAG, to underline the difference with the functionalized sample. The decomposition profile is characterized by three main steps, in the following temperature ranges: below 150°C, from 150°C to 700°C and above 700°C. Low molar mass substances, mainly water, could be responsible for the mass loss at $T < 150°C$. Decomposition of the organic part in CA–SP, arising from functionalization with SP, should occur in the temperature range from 150°C to 700°C. Also, decomposition of alkenylic groups, present as defects in HSAG, should be in this temperature range. Combustion with oxygen occurs at $T > 700°C$. Pristine HSAG washed with acetone revealed a small mass loss (0.5%) in the temperature range between 150°C and 700°C (attributed to alkenylic defects). All the three carbon allotropes show appreciable mass losses in the temperature range from 150°C to 700°C, thus confirming the occurring of functionalization.

The functionalization yield was estimated through the following equation (Equation 3):

$$\text{Functionalization Yield} = 100 \cdot \frac{\text{SP mass \% in (CA} - \text{SP adduct) after acetone washing}}{\text{SP mass \% in (CA} - \text{SP adduct) before acetone washing}} \tag{3}$$

Table 4. Mass loss for carbon allotropes functionalized with SP, from TGA analysis
Tabela 4. Strata masy alotropów węgla funkcjonalizowanych SP, na podstawie analizy TGA

Sample	Mass loss [%]			
	$T < 150°C$	$150°C < T < 400°C$	$400°C < T < 700°C$	$T > 700°C$
HSAG[a]	0.0	0.1	0.4	99.5
HSAG[b]	0.4	4.1	6.0	89.5
CB	0.2	2.9	5.3	91.6
CNT	0.4	2.4	6.8	90.4

[a]pristine sample
[b]after the reaction

Table 5. Yield of functionalization of carbon allotropes with SP[a]
Tabela 5. Wydajność funkcjonalizowania alotropów węgla za pomocą SP[a]

Carbon allotrope	Surface area	Yield of functionalization
HSAG	330	96%
CB	77	82%
CNT	275	92%

[a] from TGA analysis (see Table 4)

As already reported, % mass of SP in CA–SP adducts (before and after acetone washing) were obtained from TGA analysis, as the mass loss in the temperature range from 150°C to 700°C. Data on functionalization yield are in Table 5.

Data in Table 5 suggest that larger functionalization yield was obtained with carbon allotropes with larger surface area. However, it is indeed worth observing that the yield was high for all the three allotropes and was almost quantitative for HSAG.

Results shown so far allow to comment that functionalization reactions were successful with all the adopted methods and allowed to introduce, on the carbon allotropes, appreciable numbers of functional groups, whose nature was qualitatively investigated by means of infrared analysis. Comparative analysis is shown in the following section for HSAG as the carbon allotrope. Infrared spectra of pristine HSAG and functionalized HSAG are shown in Figure 6.

All the spectra in Figure 6 are characterized by an increasing background toward high wave numbers due to diffusion/reflection phenomena of the IR light by the particles of the sample. The spectrum of HSAG (Fig. 6a) is characterized by the band at 1590 cm^{-1} which is the peak of graphite and graphene materials, assigned to E_{1u} IR active mode of collective C=C stretching vibration.

In the spectrum of HSAG–SP (Fig. 6b), there are bands which cannot be attributed to HSAG. The broad band at 3370 cm^{-1} could be attributed to hydrogen bonded OH groups. Bands centered at about 2900 cm^{-1} are typical of sp^3 C–H stretching. Band due to diol vibration is at 1383 cm^{-1}. Stretching related to amidic C=O is at 1652 cm^{-1} and vibration of the alkenyl groups absorbs at 802 cm^{-1}. Bands in the region of C–C bonds, at 1590 and 1470 cm^{-1}, could arise from the aromatic rings.

Also in the spectrum of G–Ox sample (HSAG reacted with H_2O_2) (Fig. 6c), the C=C peak is present, along with the following broad bands, which were not detected in
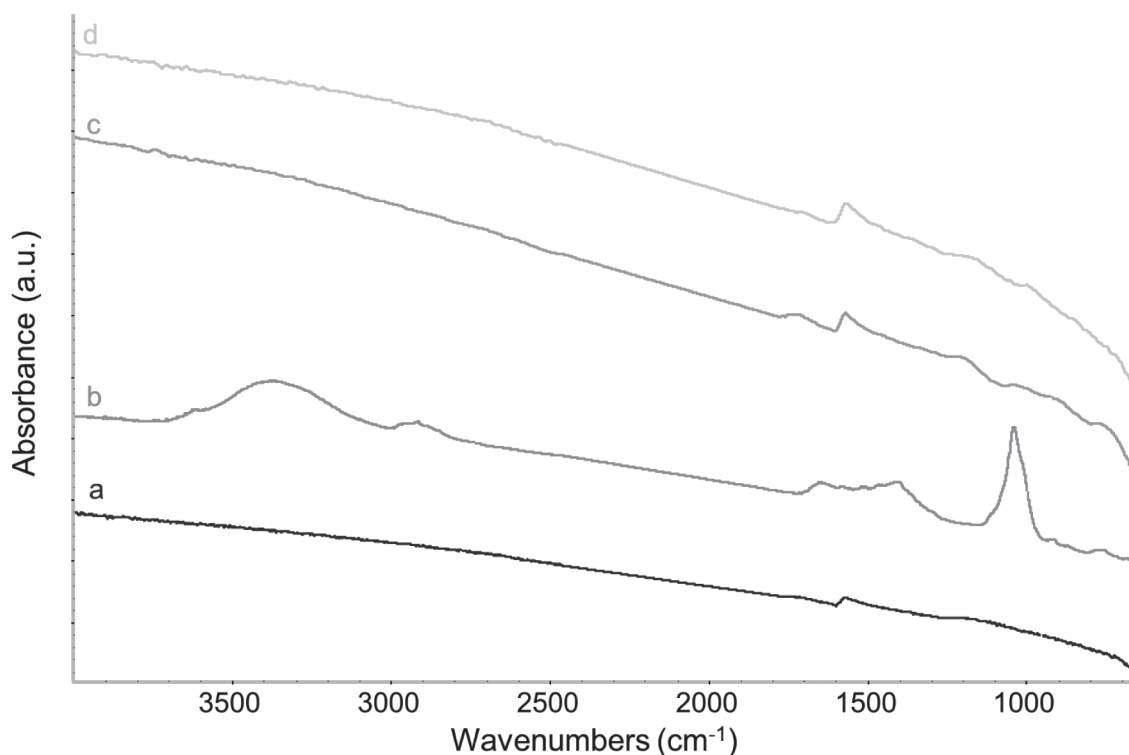
Fig. 6. FT-IR spectra of HSAG (a), HSAG–SP (b), G–Ox (c) and G–OH (d)
Rys. 6. Widma FT-IR: HSAG (a), HSAG–SP (b), G–Ox (c) i G–OH (d)

the spectrum of pristine HSAG: at 3400 cm⁻¹, a broad band related to stretching vibration of –OH; at 1388 cm⁻¹, assigned to the out of plane vibration –OH groups; at 1724 cm⁻¹, assigned to C=O stretching vibration. Other strong and broad features occurring at 1202 cm⁻¹ and 1044 cm⁻¹ can be assigned to the C–O–C bond stretching of ester and epoxide groups respectively, together with other vibrations of C–O–C and –OH functionalities.

In the spectrum of G–OH (HSAG reacted with KOH) (Fig. 6d) new bands are visible and can be assigned to the absorption of different –OH groups bonded to the graphene sheets. The corresponding peaks are located at: 3400 cm⁻¹, assigned to the –OH stretching vibrations of hydrogen bonded hydroxyl groups; 1388 cm⁻¹, assigned to the out of plane vibration –OH groups; 1110 cm⁻¹, assigned to C–O stretching vibration and 970 cm⁻¹, assigned to the in-plane phenyl–O–H bending.

The Raman spectra of HSAG, HSAG–SP, G–Ox and G–OH (recorded with the laser excitation at 632.8 nm), are reported in Fig. 7.
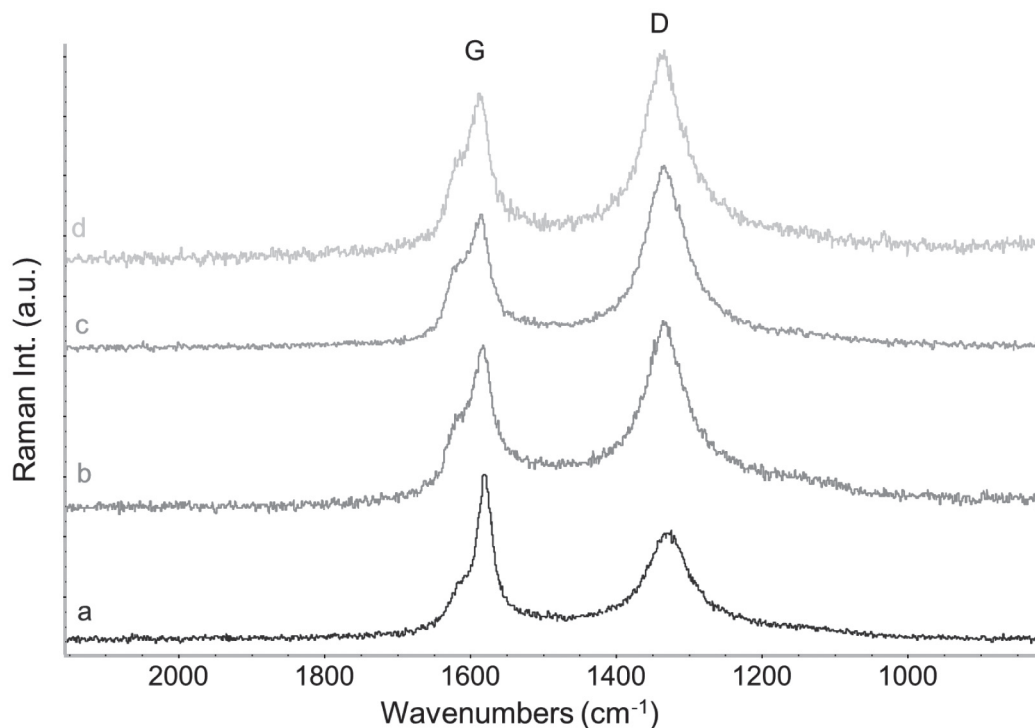

Fig. 7. Raman spectra with normalized intensities of HSAG (a), HSAG–SP (b), G–Ox (c) and G–OH (d)
Rys. 7. Widma Ramana o znormalizowanych intensywnościach: HSAG (a), HSAG–SP (b), G–Ox (c) i G–OH (d)
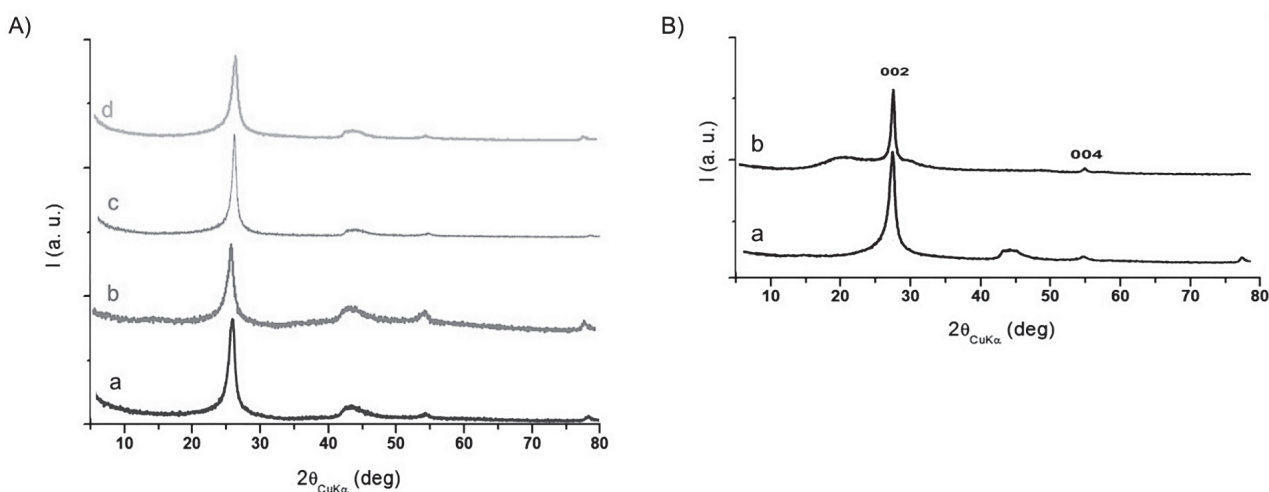
Fig. 8. WAXD patterns of: (A) HSAG (a), HSAG–SP (b), G–Ox (c) and G–OH (d). (B) Comparison between WAXD patterns of G–OH (a) and NR–GOH_15 (b)
Rys. 8. Widma szerokokątowej dyfrakcji rentgenowskiej (WAXD): (A) HSAG (a), HSAG–SP (b), G–Ox (c) and G–OH (d). (B) Porównanie widm WAXD G–OH (a) i NR–GOH 15 (b)

The presence of graphitic sp^2-phase in the Raman spectra is mainly revealed by two main peaks located at 1580 cm^{-1} and 1350 cm^{-1} named G and D, respectively [43, 44]. G and D bands are present in all spectra, with similar intensity. The high intensity of the D band can be due to the different types of molecular disorder. However, there are not indications that the reaction of HSAG with each oxidizing agent appreciably alter the structure of the graphitic layers.

Figure 8A shows WAXD patterns taken on powders of HSAG (Fig. 8Aa), HSAG–SP (Fig. 8Ab), G–Ox (Fig. 8Ac) and G–OH (Fig. 8Ad).

In pristine HSAG, crystalline order in the direction orthogonal to structural layers is revealed by two (001) reflections: 002 at 26.6°, that corresponds to an interlayer distance of 0.338 nm and 004 at 54.3°. The in-plane order is shown by 100 and 110 reflections, at 42.5° and 77.6° respectively. Peak shape analysis was applied to (002) reflection and size of crystallites was calculated by means of the Scherrer equation (see the Experimental part). It was found that the procedure adopted for oxidizing HSAG led to the reduction of crystallites' size. Indeed, the following values were obtained for the number of stacked layers: 35 in HSAG, 24 in HSAG–SP, 28 in G–Ox and 23 in G–OH. 100 and 110 reflections are clearly visible in each pattern. From these findings, it can be commented that the reaction with SP, H$_2$O$_2$ and KOH promotes the partial exfoliation of HSAG without altering the in-plane order.

3.2. Composites with functionalized carbon allotropes

In the text below, are reported composites based on functionalized carbon allotropes, prepared either via latex or melt blending, with NR, IR and BR as the rubbers and carbon black and silica as the fillers.

In particular, G–OH was used as the only filler in composites based on NR, prepared via latex blending. CB–SP was used in composites based on IR and BR with CB and silica as the filler system.

3.2.1. Composites based on NR and G–OH

Composites based on NR and G–OH were prepared as described in the experimental part. Recipes are in Table 1. Structure of the composites was investigated by means of TEM and WAXD analyses. Figure 9 shows the TEM micrographs of the composite NR–GOH_9 as precipitated from the latex.

G–OH appears to be evenly distributed. Aggregates of G–OH of sub-micrometric size and few agglomerates not larger than 3 µm are visible at low magnification (Fig. 9a). Very few isolated graphene layers and stacks of layers, of different dimensions, can be seen in the micrograph at high magnification (Fig. 9b): some of the stacks contain only few layers.

WAXD analysis was taken on crosslinked NR–GOH_15 composite, which contained 15.1 phr of G–OH. In Figure 8B were reported patterns of G–OH (Fig. 8Ab and Fig. 8Ba) and NR–GOH_15 (Fig. 8Bb). (002) reflection remains at the same 2θ value in the pattern of the elastomer composite, indicating that the oxidation reaction did not promote expansion of the interlayer distance. The number of graphene layers stacked in GOH in the composite was calculated by applying the Scherrer equation (see the Experimental part), as done above for pristine HSAG and for G–OH. The following value was obtained: 66 (35 and 23 were in pristine HSAG and in G–OH). Hence, it seems that the procedure of reaggregation of G–OH layers into a crystalline domain occurred when the composite was vulcanized. Some of the authors reported [21] that the number of layers stacked in crystalline HSAG
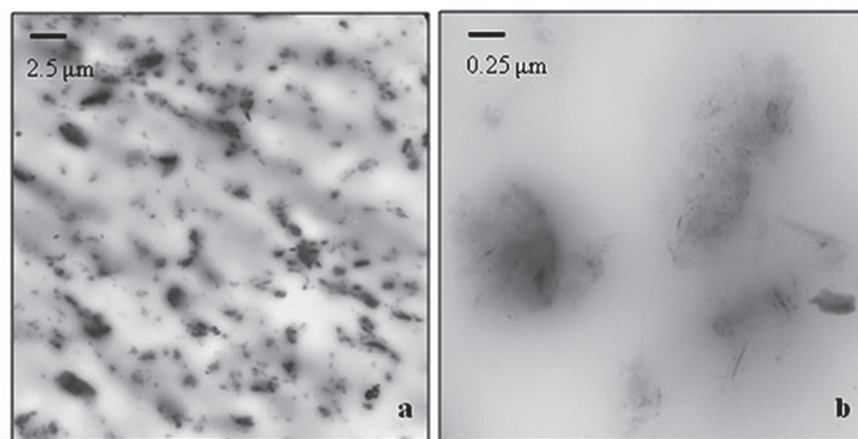

Fig. 9. TEM micrographs of NR–GOH–9 composite, as precipitated from the latex, at low (a) and high (b) magnifications
Rys. 9. Mikrofotografie kompozytu NR–GOH–9, w małym (a) i dużym powiększeniu (b)

domains increased from about 35 to about 70, passing from pristine HSAG to the vulcanized composite. It appears reasonable to comment that the energy given to the composite during the vulcanization step brings graphene stacks to the minimum of energy, that means to the crystalline organization.

Crosslinking of the composites was performed with a sulphur-based system. Data taken from the rheometric curves are in Table 6.

From the data in Table 6, it appears that M_L values, which are a viscosity index, increased by increasing the amount of G–OH in the composite. The induction time of vulcanization is revealed by t_{s1} parameter. t_{s1} values were also normalized with respect to t_{s1} values of the matrix and were plotted as a function of the G–OH content. Graph is shown in Figure 10.

It is evident that the induction time of vulcanization consistently decreases by enhancing the amount of G–OH in the composite. In the literature, it was reported

that faster vulcanization reactions are promoted by carbon allotropes [40].Graph in Figure 11 reports M_H and $(M_H – M_L)$ values as a function of the G–OH content: as expected M_H values consistently increase by enhancing the content of G–OH.

The linear increase of M_H with G–OH content (at least up to 15.1 phr as G–OH content), suggests that G–OH was evenly dispersed in the NR matrix. This comment is substantially in line with what shown by TEM micrograph shown in Figure 9. The minor increase of M_H passing from 15 phr to 25 phr as G–OH content (see Table 6) can be explained with the unsatisfactory incorporation of G–OH in the NR matrix. All the results from rheometric tests can be correlated with the amount of G–OH in the composites. In particular, from the graph in Figure 10, it appears that values from G–OH based composites can be normalized with respect to values of composite based on pristine HSAG. Hence, there are no indication of any effect by the functional groups.

Table 6. Data from crosslinking reactions of composites based on NR and G–OH
Tabela 6. Dane dotyczące reakcji sieciowania kompozytów opartych na NR i G–OH

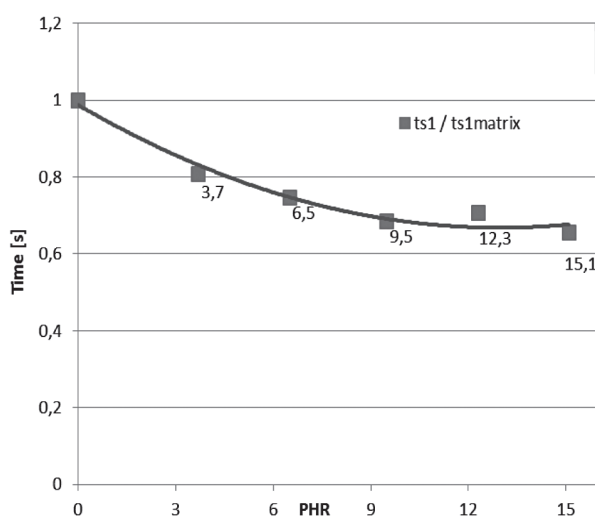| Parameter	Composite						
	G-OH_0	**G-OH_4**	**G-OH_7**	**G-OH_10**	**G-OH_12**	**G-OH_15**	**G-OH_25**
M_L	0.4	0.3	0.3	0.4	0.4	0.5	0.7
M_H	9.6	10.8	10.9	11.4	12.0	12.5	13.8
t_{s1}	4.3	3.4	3.2	2.9	3.0	3.0	3.3
t_{90}	8.2	7.6	7.2	6.8	7.3	7.3	8.9

Fig. 10. $t_{s1}/t_{s1matrix}$ vs G–OH content (phr) for the crosslinking reactions of composites of Table 1
Rys. 10. Zależność $t_{s1}/t_{s1matrix}$ od zawartości G–OH (phr) dla reakcji sieciowania kompozytów z Tabeli 1
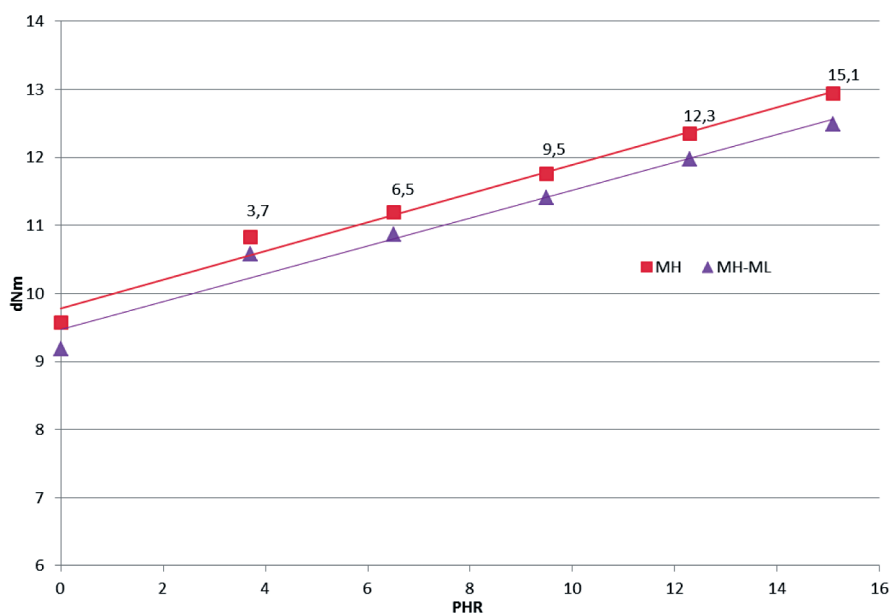
Fig. 11. M_H and $(M_H - M_L)$ as a function of G–OH content for the crosslinking reactions of composites of Table 6
Rys. 11. M_H i $(M_H - M_L)$ w funkcji zawartości G–OH dla reakcji sieciowania kompozytów z Tabeli 6
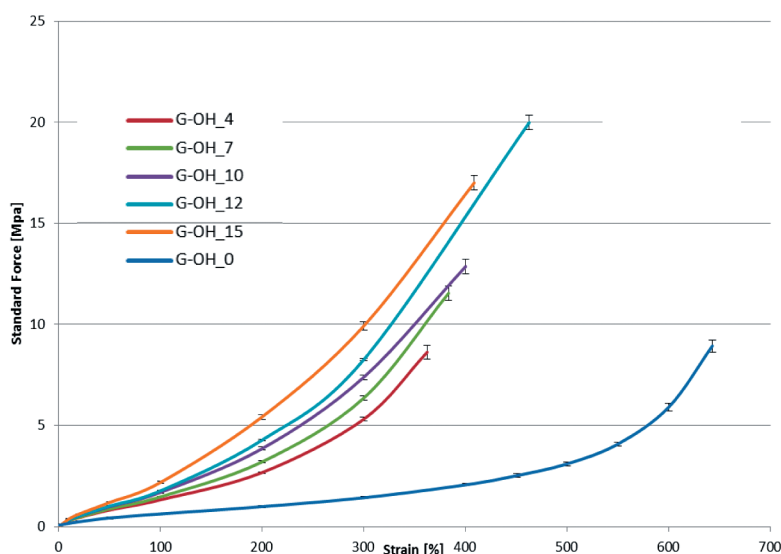

Fig. 12. Nominal stress–nominal strain curves, with standard deviations, obtained for crosslinked G–OH composites of Table 1
Rys. 12. Krzywe nominalne naprężenie – nominalne wydłużenie, ze standardowymi odchyleniami, otrzymane dla usieciowanych kompozytów z Tabeli 6

Tensile measurements were carried out on crosslinked composites, by applying uniaxial stretching, as described in the Experimental part. The graph shown in Figure 12 shows the dependence of nominal stress on nominal strain.

The lowest values of stresses at every elongation and the largest deformation were obtained for neat NR. G–OH led to the increase of stresses and to the reduction of strain at break. Stresses appear to increase consistently with G–OH content. The ultimate properties of NR-GOH_15 were found to be slightly lower than those of NR-GOH_12: this could be attributed to the presence of agglomerates of G–OH.

3.2.2. Composites based on IR, BR and CB–SP

Composites containing CB–SP were prepared, based on IR and BR as the rubbers and CB and silica as the

fillers. Objective was to reduce the silica filler networking thanks to the silica interaction with functionalized CB. Recipes are shown in Table 2 in the Experimental section. The same CB amount was used: SP (1:10 by mass with respect to CB) was thus an extra-ingredient in the composite. Crosslinking was performed with a sulphur-based system. Rheometric curves, taken at 170°C and shown in Figure 13, do not reveal significant differences of vulcanization kinetic: induction time (t_{s1}) and the time request to achieve the optimum of vulcanization time (t_{90}) were found to be very similar.

It is worth recalling that on CB are present hydroxy groups and a basic nitrogen, which could promote a faster vulcanization. At the explored SP content, this is not observed. It can be thus commented that the treatment with SP does not modify the effect of CB on the crosslinking kinetics. The use of CB–SP leads to slightly lower levels of M_H.

To investigate filler networking phenomenon, strain sweep experiments were performed at 50°C, on crosslinked samples. The dependence of shear storage modulus G' on strain amplitude is shown in Figure 14A and the dependence of G'' on G' is shown in Figure 14B.

The addition of CB–SP leads to the reduction of the Payne Effect [46]. As it appears from the Cole-Cole plot in Figure 14B, for a given level of dynamic stiffness, the use of CB–SP allows to have lower loss modulus.

4. Conclusions

This paper shows that carbon allotropes such as a nanosized graphite, carbon black and carbon nanotubes can be functionalized, without substantially altering their bulk crystalline structure. KOH, hydrogen peroxide and a serinol derivative, serinolpyrrole,
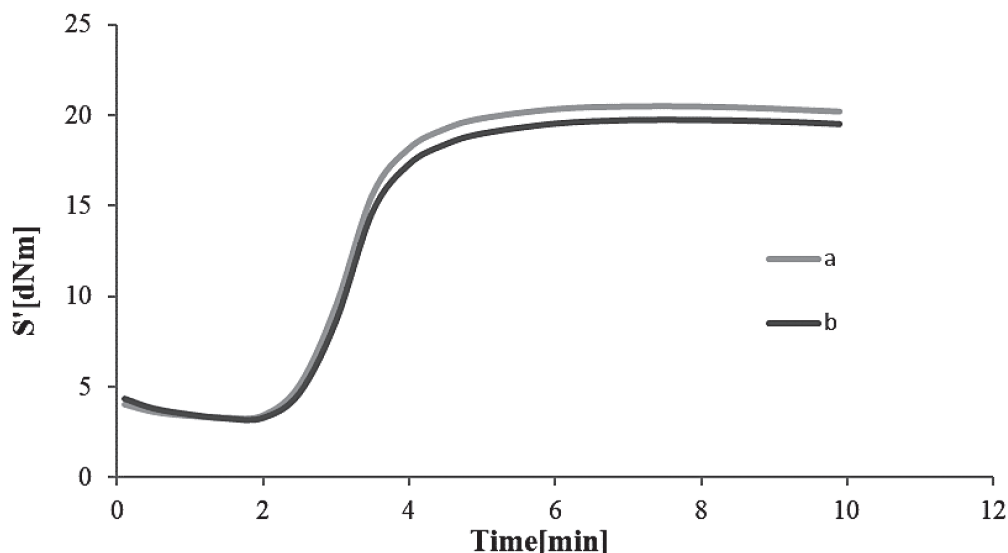

Fig. 13. Rheometric curves obtained at 170°C for composites of Table 2. Content of CB–SP: a) 0 phr; b) 5.5 phr
Rys. 13. Krzywe reometryczne otrzymane w 170°C dla kompozytów z Tabeli 2. Zawartość CB–SP: a) 0 phr; b) 5,5 phr
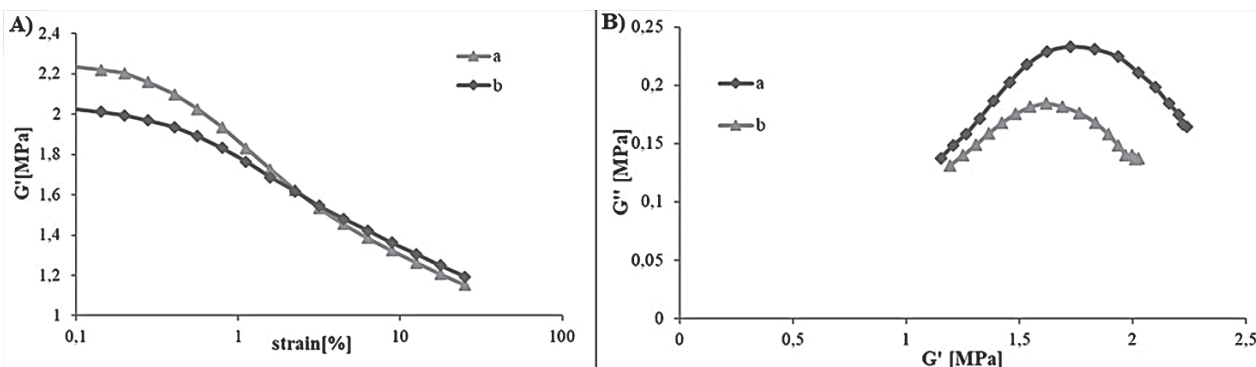

Fig. 14. (A) Dynamic storage modulus G' [MPa] versus strain amplitude [%], (B) loss modulus G'' [MPa] versus storage modulus G' [MPa], for composites of Table 2. Content of CB–SP: a) 0 phr; b) 5.5 phr
Rys. 14. (A) Dynamiczny moduł zachowawczy G' [MPa] w funkcji amplitudy odkształcenia [%], (B) moduł stratności G'' [MPa] w funkcji modułu zachowawczego G' [MPa], dla kompozytów z Tabeli 2. Zawartość CB–SP: a) 0 phr; b) 5,5 phr

were used as the functionalizing agents. Reactions were performed in the absence of catalyst and by simply donating either thermal or mechanical energy. Appreciable number of oxygenated groups were added to the carbon allotropes. In particular, with serinolpyrrole, about 10% of functional group were detected on HSAG and the yield of functionalization was high for all of the carbon allotropes, higher than 90% for CB and HSAG. Elastomer composites were prepared with functionalized carbon allotropes. HSAG oxidized with KOH gave better tensile properties to NR based composite from latex blending than HSAG in analogous composites from melt blending. Filler networking phenomenon in silica based composites can be reduced with CB modified with SP.

References

1. Wang M.J., Gray C.A., Reznek S.A., Mahmud K., Kutsovsky Y., *Carbon Black*, Kirk-Othmer *Encyclopedia of Chemical Technology* (2003).
2. Voet A., Morawski J.C., Donnet J.B., *Rubber Chem. Technol.*, 1977, **50**, 342.
3. Maiti M., Bhattacharya M., Bhowmick A.K., *Rubber Chem. Technol.*, 2008, **81**, 384.
4. Paul D.R., Robeson L.M., *Polymer*, 2008, **49**, 3187.
5. Galimberti M., Cipolletti V., Musto S., Cioppa S., Peli G., Mauro M., Guerra G., Agnelli S., Riccò T., Kumar V., *Rubber Chem. Technol.*, 2014, 87,**417,** 3.
6. Galimberti M., Cipolletti V., Coombs M., "Applications of Clay–Polymer Nanocomposites" in *Handbook of Clay Science*, Elsevier, 2013.
7. Bokobza L., *Polymer*, 2007, **48**, 4907.
8. Bhattacharya M., Maiti M., Bhowmick A.K., *Polymer Engineering & Science*, 2009, **49**, 81.
9. Bhowmick A.K., Bhattacharya M., Mitra S., *J. Elastomers Plast.*, 2010, **42**, 517.
10. Al-Solamya F.R., Al-Ghamdib A.A., Mahmou W.E., *Polymer Adv. Technol.*, 2012, **23**, 478.
11. Galimberti M., Kumar V., Coombs M., Cipolletti V., Agnelli S., Pandini S., Conzatti L., *Rubber Chem. Technol.* 2014, **87**, 197.
12. Maiti M., Bhattacharya M., Bhowmick A.K., *Rubber Chem. Technol.*, 2008, **81**, 384.
13. Paul D.R., Robeson L.M., *Polymer*, 2008, **49**, 3187.
14. Galimberti M., Cipolletti V., Musto S., Cioppa S., Peli G., Mauro M., Guerra G., Agnelli S., Riccò T., Kumar V., *Rubber Chem. Technol.,* 2014, 87, **417**, 3.
15. Terrones M., Botello-Méndez A.R., Campos-Delgado J., López-Urías F., Vega-Cantú Y.I., Rodríguez-Macías F.J., Terrones H, *Nano Today*, 2010, **5**, 351.
16. Zhang J., Terrones M., Park C.R., Mukherjee R., Monthioux M., Koratkar N., Kim Y.S., Hurt R., Frackowiak E., Enoki T., Chen Y., Chen Y., Bianc A., *Carbon*, 2016, **98**, 708–732.
17. Galimberti M., Coombs M., Riccio P., Riccò T., Passera S., Pandini S., Conzatti L., Ravasio A., Tritto I., *Macromol. Mater. Eng.*, 2012, **298**, 241–251.
18. Galimberti M., Coombs M., Cipolletti V., Riccò T., Agnelli S., Pandini S., *KGK (Kautschuk Gummi Kunstoffe)*, 2013, **7–8**, 31–36.
19. Galimberti M., Kumar V., Coombs M., Cipolletti V., Agnelli S., Pandini S., Conzatti L., *Rubber Chem. Technol.*, 2014, **87**, 2, 197–218.
20. Galimberti M., Agnelli S., Cipolletti V., *Progress in Rubber Nanocomposites,* 1st Edition, Sabu Thomas Hanna Maria, Woodhead Publishing, 2016.
21. Agnelli S., Cipolletti V., Musto S., Coombs M., Conzatti L., Pandini S., Riccò T., Galimberti M., *eXPRESS Polymer Letters*, 2014, **8**(6), 436.
22. Agnelli S., Pandini S., Serafini A., Musto S., Galimberti M., *Macromolecules*, 2016, **49**(22), 8686–8696.
23. Agnelli S., Pandini S., Torricelli F., Romele P., Serafini A., Barbera V., Galimberti M., *eXPRESS Polymers Letters*, accepted for publication.
24. Galimberti M., Barbera V., Guerra S., Bernardi A., *Rubber Chem. Technol.*, 2017, **90**(2), 285–307.
25. Galimberti M., Barbera V., Sironi A., *Graphene Materials – Structure, Properties and Modifications,* 2017, Dr. George Kyzas (Ed.), InTech, DOI: 10.5772/67630.
26. Donnet J.B., *Carbon black: science and technology*, 1993.
27. Wang M.J., Kutsovsky Y., Zhang P., Murphy L.J., Laube S., Mahmud K., 2002, **75**, 247.
28. Wang M.J., Mahmud K., Murphy L.J., Patterson W.J., *Kautschuk Gummi Kunststoffe*, 1998, **51**, 348.
29. Wang W., Vidal A., Donnet J.B., Wang M.J., *Kautschuk Gummi Kunststoffe*, 1993, **46**, 933.
30. Kinney C.R., Friedman L.D., *J. Am. Chem. Soc.*, 1952, **57**, 74.
31. Cines M.R., *Can. Pat.*, 1956, **9**, 531.
32. Rodriguez J., Ghosal R., Narayanan S.K., WO 2013098838 A3, 2013.
33. Cataldo F., *Journal of nanoscience and nanotechnology*, 2007, **7**, 1446.
34. Wampler W., Jacobsson B.M., Nikiel L., Cameron P.D., Neilsen J., US20150191579, 2015.
35. Belmont J.A., Tirumala V.R., Zhang P., WO 2013130099, 2013.
36. Park S.J., K.S. Cho K.S., Ryu S.K., *Carbon*, 2003, **41**(7), 1437–1442.
37. Gozdek R., Sicinski M., Bielinski D.M., Okraska M., Szymanowski H., Piatkowska A., *Elastomery*, 2017, **21**(1), 12–19.
38. Mauro M., Cipolletti V., Galimberti M., Longo P., Guerra G., *J. Phys. Chem.*, 2012, C**116**, 24809.
39. Andreeßen B., Steinbüchel A., *AMB Express*, 2011, **1**, 1.
40. Musto S., Barbera V., Cipolletti V., Citterio A., Galimberti M*., eXPRESS Polymer Letters*, 2017, **11**(6), 435–448.
41. Knorr L., *Chem. Ber.*, 1885, **18**, 299.
42. Paal C., *Chem. Ber.*, 1885, **18**, 367.
43. Barbera V., Porta A., Brambilla L., Guerra S., Serafini A., Valerio A.M., Vitale A., Galimberti M., *RSC Adv.*, 2016, **6**, 87767–87777.
44. Galimberti M., Barbera V., Guerra S., Conzatti L., Castiglioni C., Brambilla L., Serafini A., *RSC Adv.*, 2015, **5**, 81142.
45. Barbera V., Bernardi A., Palazzolo A., Rosengart A., Brambilla L., Galimberti M., *Pure Appl. Chem.,* 2017, DOI: https://doi.org/10.1515/pac-2017-0708.
46. Payne AR., Whittaker R.E., *Rubber Chem. Technol.*, 1971, **44**, 440–478.